Journal of Alloys and Compounds, 207/208 (1994) 146–152
JALCOM 3095

Microscopic parameters of R–T hard magnets

M. Loewenhaupt and P. Fabi
Institut für Festkörperforschung, Forschungszentrum Jülich, D-52425 Jülich (Germany)

Abstract

R–T compounds with R = rare earth and T = transition metal have become the most important materials in modern hard magnet technology. The unusual magnetic properties of these materials originate from the interplay between the strong crystal field anisotropy of the R atoms and the large magnetization and exchange interaction of the T atoms. Inelastic magnetic neutron scattering can be employed to determine some relevant microscopic parameters of magnetic compounds. We discuss a case where the crystal field interaction dominates the exchange interaction ($NdCu_2$, an intermetallic compound with low magnetic ordering temperature) and compare it to the situation in R–T hard magnets where the exchange interaction $\mathcal{J}_{RT}$ is much stronger than the crystal field interaction. We discuss the experimental results for RFe_2 and $R_2Fe_{14}B$ compounds and compare the microscopic parameters as deduced from different experimental methods and from *ab initio* calculations.

1. Introduction

Since the discovery of NdFeB-type magnets [1], there has been increasing interest in improving understanding of the physical mechanisms that determine the intrinsic magnetic properties of these materials. Superior intrinsic properties are an indispensible precondition to achieving superior performance of a new hard magnetic material. The main technological problem, however, is to produce an adequate microstructure (grain size, defects, impurity phases) to fully exploit the intrinsic magnetic properties. Here, however, we will concentrate on the description of the relevant intrinsic parameters on an atomic scale, the microscopic parameters, and their determination by different experimental methods. The experimental values are then compared with those obtained from *ab initio* band structure calculations.

The main requirements for a high-performance hard magnet are: a large magnetization and a high coercive force to obtain a large "energy product" and a high Curie temperature to warrant safe operation at room temperature and at elevated temperatures as high as possible. The recipe for obtaining the desired magnetic properties is to form R–T compounds with R = rare earth and T = transition metal. The strong anisotropy of the unquenched orbital part of the R-moments delivers the asset for the high coercive force (in connection with the adequate microstructure) while the transition metal (Fe or Co) is responsible for a sufficiently high magnetization and Curie temperature. Finally, the R–T coupling should be strong enough to transfer the individual magnetic properties between both subsystems. There is, however, one severe drawback in the considerations outlined above. The R–T coupling is always negative for the spin part of the magnetic moments. Thus, the large total magnetic moments $J = L + S$ of the heavy rare earths point in the opposite direction of the T-moments and thus reduce the total magnetization of a heavy rare earth T compound. Therefore, only the light rare earth T compounds are of technical importance (like *e.g.* $SmCo_5$, $Nd_2Fe_{14}B$). For the light rare earths, the third Hund's rule yields $J = L - S$ for the ground state multiplet. The negative spin spin coupling then produces a ferromagnetic alignment of the total magnetic moment of the light rare earth with the Fe or Co moments which are dominantly of spin character. The residual orbital magnetism of Fe or Co also gives rise to anisotropic behavior but the anisotropy of the T-component is usually much weaker than the anisotropy of the R component. In this connection, one has to keep in mind that R = Y, La or Lu (and often also Ce) are considered as non-magnetic while R = Gd has a spin-only moment (half filled f-shell with $L = 0$ and $J = S = 7/2$). This implies that these R-ions show isotropic behavior and do not contribute to any anisotropy. If anisotropy is observed experimentally in such materials, it is attributed to the T component.

This paper is organized as follows: first we discuss the case where the crystal field interaction is much stronger than the exchange interaction (*i.e.* in an intermetallic compound like $NdCu_2$ with no moment on the Cu-ions and a low magnetic ordering temperature of only 6.5 K). For this case, we demonstrate the power

SSDI 0925-8388(94)03095-E

of inelastic magnetic neutron scattering to determine the crystal field level scheme of systems with low local symmetry of the R-sites ("neutron crystal field spectroscopy", see *e.g.* ref. 2). We then proceed to the opposite case of the R–T hard magnets where the exchange interactions are dominant and the crystal field interaction is only a small perturbation. The crucial experiments for this case are inelastic magnetic neutron experiments on Gd–T compounds which allow the determination of the exchange constants in the absence of crystal field effects. A comparison of the experimental values with those obtained from *ab initio* band structure calculations is a good test for the liability of the theoretical predictions for the other R–T compounds. The experimental determination of the full set of crystal field parameters of the other R–T compounds is still far from being unique. Final success will only be achieved if all experimental data are considered and backed-up by a reliable theoretical input.

2. $NdCu_2$, an example for "neutron crystal field spectroscopy"

$NdCu_2$ is an intermetallic compound which has been investigated rather thoroughly [3]. It crystallizes in the orthorhombic $CeCu_2$-type structure with the space group $D_{2h}^{28}(Imma)$. There is one R-site with the local point symmetry C_{2v} and hence there are nine independent crystal field parameters to describe the CF Hamiltonian. Using the Stevens operator equivalent method [4] and the notation of Hutchings [5], these are: B_{20}, B_{22}, B_{40}, B_{42}, B_{44}, B_{60}, B_{62}, B_{64} and B_{66}. For more information on crystal fields, see *e.g.* [6–9].

As Nd^{3+} is a Kramers ion ($J=9/2$, a half integer value of J), for the given low symmetry of the Nd site in $NdCu_2$, we expect a splitting of the 10-fold degenerate ground state into 5 doublets by the action of the crystalline electric field. The ground state of a non-Kramers ion with integer value of J (like Pr, $J=4$, Tb and Tm, $J=6$, and Ho, $J=8$) can be split by a crystal field into maximal $(2J+1)$ singlets.

The crystal field level schemes can be measured directly by inelastic magnetic neutron scattering. Figures 1 and 2 show the inelastic neutron spectra of $NdCu_2$ measured at $T=10$ K in the paramagnetic state and at $T<T_N=6.5$ K in the magnetically ordered state. The value of the neutron momentum transfer Q is kept low (1–2 Å) so that magnetic scattering is the dominant contribution to the scattering intensity (except for elastic scattering). Inelastic phonon scattering is negligible in the spectra shown in Figs. 1 and 2. In the paramagnetic state, there are four inelastic magnetic transitions which can be interpreted as crystal field transitions from the ground state doublet to the four excited doublets situated at 2.9, 5.0, 7.2 and 14.1 meV above the ground state. Because of the low temperature, there are no transitions between excited states. The corresponding level scheme is shown as an inset in Fig. 1. The data points for three runs under different experimental conditions are

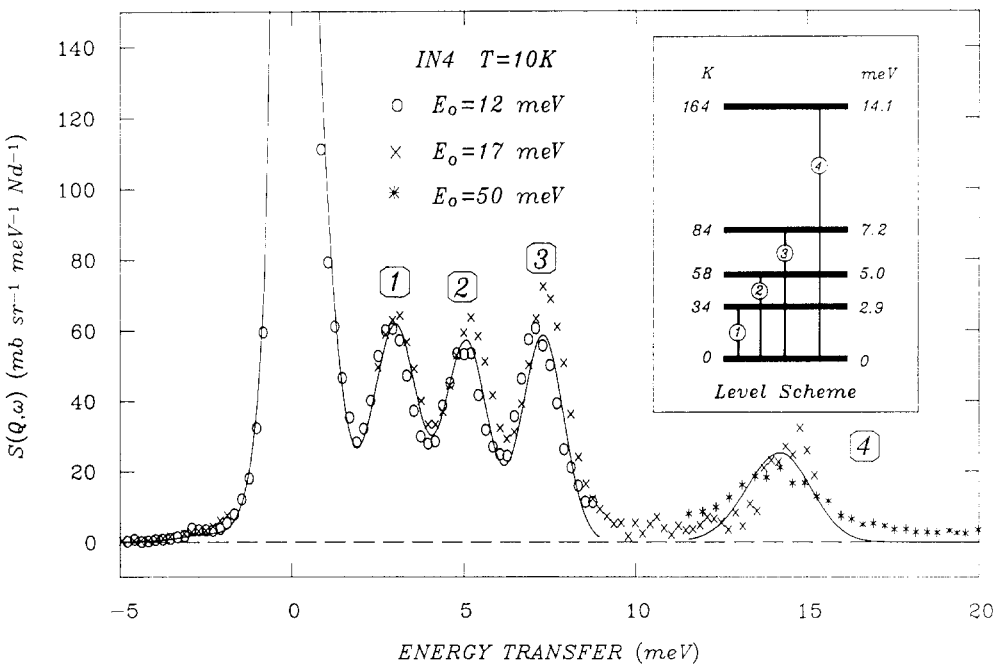

Fig. 1. Inelastic neutron spectra of $NdCu_2$ in the paramagnetic state at $T=10$ K obtained with different incident neutron energies E_0. The deduced crystal field transitions are given by the level scheme in the inset. Nine crystal field parameters have been obtained with the superposition model from these data (full curve) [3].

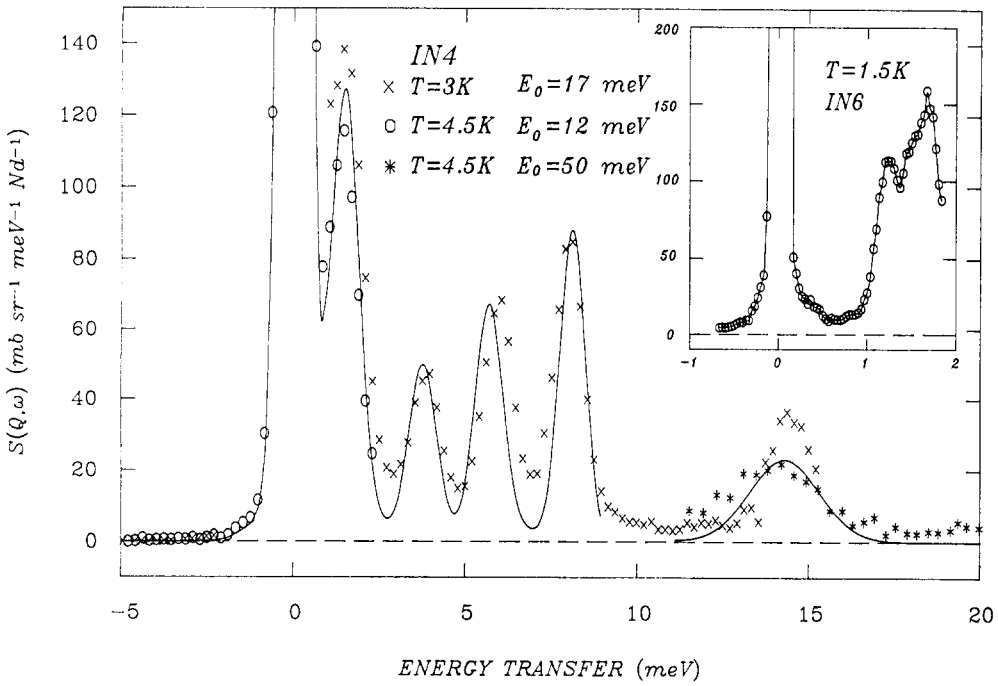

Fig. 2. Inelastic neutron spectra of $NdCu_2$ at various temperatures below the Néel temperature of 6.5 K obtained with different incident neutron energies. The inset shows the low energy region up to 2 meV measured at $T=1.5$ K on a different instrument with improved energy resolution. This low-energy intensity originates from magnon excitations. From ref. 3.

in good agreement with respect to peak positions and absolute intensities. In the magnetically ordered state, the inelastic magnetic neutron spectra as shown in Fig. 2 are modified compared to those in the paramagnetic state. With coarse resolution, we observe a splitting of the ground state doublet and a shift of the peak positions of the crystal field transitions. In a first approximation one can reproduce this inelastic spectrum by adding to the single-ion CF-Hamiltonian an internal (exchange) magnetic field term of the order of a few tesla. This simple model yields a Zeeman splitting of the doublets in the ordered state. A sketch of the situation for $NdCu_2$, the case where the crystal field interaction is much stronger than the exchange interaction, is given in Fig. 3 on the left hand side.

In reality, however, the excitation spectrum of magnetically ordered $NdCu_2$ is much more complex. This can be inferred from the measurement of the low-lying peak around 1.5 meV with improved energy resolution using a different neutron spectrometer as shown in the inset of Fig. 2. It reveals considerably more of the structure of this excitation. The intensity in the energy range up to 2 meV has therefore to be identified as a magnon density of states. A detailed investigation of the magnon dispersion relations, *i.e.* of the low-energy collective magnetic excitations in the magnetically ordered state using a single crystal of $NdCu_2$ is currently underway.

Although the crystal field level scheme of $NdCu_2$ has been determined quite accurately by neutron spec-

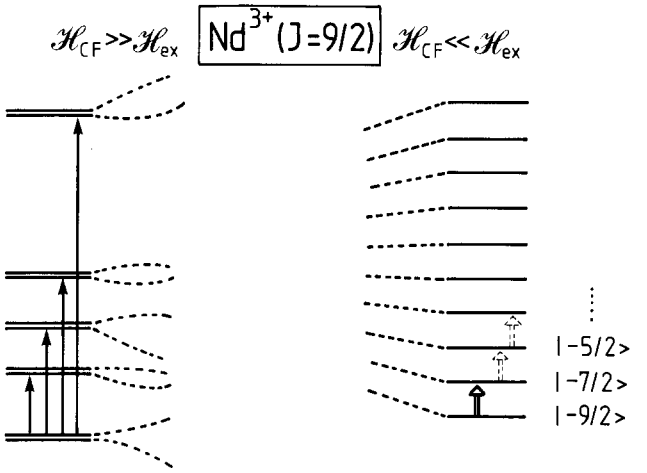

Fig. 3. Single-ion level schemes for Nd^{3+} ($J=9/2$) for the two extreme cases of dominant crystal field (left) and dominant exchange field (right).

troscopy, the determination of the nine independent crystal field parameters is another formidable task. It is very difficult because of the huge parameter space and the highly non-linear dependence between parameters and experimental data. To obtain at least preliminary results, one usually employs certain models to reduce the number of free parameters. Unfortunately, none of the models (point charge; superposition; band structure calculations) is advanced and accurate enough to lead to reliable results except for some favorable cases. Therefore, we hesitate to consider the set of

nine parameters given in [3] as final although it explains the neutron spectra quite well (full lines in Figs. 1 and 2, except for inset in Fig. 2) together with the effects of the crystal field on magnetization, specific heat, thermal expansion and resistivity data.

3. RFe_2, a simple "model case"

We now proceed to the case of R–T compounds where the exchange interactions are dominant while the crystal field is only a small perturbation. In this section, we first consider a simple model case: the cubic Laves phase (C15) compounds RFe_2. The spin dynamics were investigated by inelastic neutron scattering on single crystals with R = Tb, Ho and Er some years ago [10–12]. The outcome of these investigations was that there is a hierarchy of exchange interactions:

$$\mathcal{J}_{FeFe} \gg \mathcal{J}_{RFe} \gg \mathcal{J}_{RR}$$

This leads to a characteristic picture of the spin wave dispersion relations as sketched in Fig. 4 for the low-energy region. From the total of six modes (the unit cell contains two formula units with two R and four Fe magnetic ions), there are three low lying modes. Two of them are dispersive: one is an in-phase acoustic mode involving all spins with a dispersion roughly given by the R–T exchange (dashed line) and the other mode is a highly dispersive in-phase mode involving only Fe spins with a spin wave stiffness constant similar to that of Fe-metal (thin line). The third low lying mode is a flat mode corresponding to an out-of-phase precession of the R-spins in the exchange field of the surrounding Fe-spins (thick line). In the following, we mainly concentrate on that mode. For $\mathcal{J}_{RR} = 0$, the latter mode is completely flat (dispersionless). For an isotropic Heisenberg-model with nearest-neighbor exchange, there is no spin wave gap at the Γ-point for the low-lying dispersive mode. The energy Δ of the flat R-mode is given by

$$\Delta = 2z_{RT}|g_R - 1|\mathcal{J}^{ex}_{RT} S_T = 2z_{RT}\mathcal{J}_{RT} S_T \quad (1)$$

with z_{RT} = number of T-neighbors of a R-ion (12 for RFe_2) and S_T = spin of T-ions. Alternatively, the flat mode energy can be related to an exchange or molecular field by

$$\Delta = 2\mu_B|g_R - 1|B^{ex} = \mu_B g_R B^m \quad (2)$$

with g_R = Landé factor of the R ion and the Bohr magneton $\mu_B = 0.05788$ meV/T. Note the different definitions of exchange constants and internal fields, respectively. This situation is illustrated for Nd^{3+} with $J = 9/2$ in Fig. 3 on the right-hand side. For pure Zeeman splitting, all 10 levels are equally spaced with separation Δ between adjacent levels. Inelastic magnetic neutron scattering has only finite matrix elements between adjacent levels (dipole transitions). For low temperatures, only the ground state level is populated. The flat mode can then be viewed as the transition from the ground state to the first excited state. At elevated temperatures, transitions between excited levels (dashed arrows in Fig. 3) will also be observed.

Adding a small crystal field term to the Zeeman term results in the following modifications of the level scheme: (i) the levels are no longer equally spaced; (ii) the wave functions become linear combinations of the pure Zeeman states; and (iii) transitions between non-adjacent levels are also allowed although with typically much smaller matrix elements. In this situation, it is not possible to determine $\mathcal{J}_{RT}$ or B^{ex} directly from the energy Δ of the flat mode. Instead, the full Hamiltonian, including $\mathcal{H}_{CF}$ and $\mathcal{H}_{ex}$ has to be diagonalized. This, of course, requires the knowledge of the correct set of crystal field parameters if one wants to deduce the R–T exchange from Δ. Furthermore, the action of the crystal field on the R-ions may introduce an anisotropy which becomes visible as a gap of the lowest dispersion curve at the Γ-point. All these considerations were taken into account when analyzing the inelastic neutron data of RFe_2 with R = Tb, Ho and Er [10] (because of the cubic symmetry there are, however, only two CF-parameters to be determined). The values deduced for $\mathcal{J}^{ex}_{RT}$ are shown at the end of this section in Fig. 6 together with those from other experiments and from calculations.

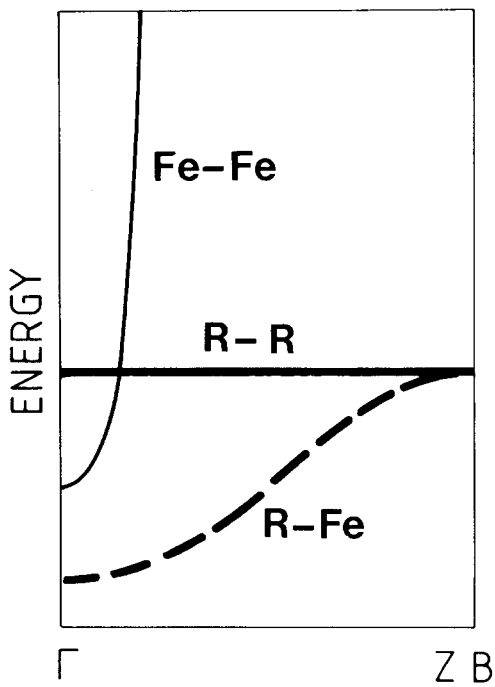

Fig. 4. Dispersion relations for the three low-lying magnon branches of a mixed R–Fe compound (see *e.g.* ref. 10).

We now present the results of inelastic neutron scattering experiments on $GdFe_2$ which can be interpreted within the simple considerations discussed above for pure Zeeman splitting and expressed in eqns. (1) and (2). For this purpose, a polycrystalline sample is sufficient to observe an excitation spectrum which will show as its dominant contribution a pronounced peak due to the flat mode, while the dispersive modes will only give a smooth, low intensity contribution to the background. Unfortunately, natural Gd is the strongest thermal neutron absorber of all elements and low absorbing Gd-isotopes are extremely expensive (typically \$5 per mg). The neutron absorption cross-section of natural Gd, however, is strongly energy dependent and is considerably reduced for neutron energies above about 200 meV. A good compromise to achieve a reasonable energy resolution (small E_0) and to obtain sufficient intensity (high E_0 for low absorption) is an incident neutron energy E_0 of 250 meV. The best suited time-of-flight spectrometer for this purpose is the HET instrument situated at the ISIS neutron spallation source of the Rutherford Appleton Laboratories. Figure 5 shows the neutron spectrum for $GdFe_2$ measured at $T=12$ K [13]. The peak at an energy transfer of $\Delta=(44\pm1)$ meV can be easily identified as the Gd-flat mode. From eqn. (2) and with $g_{Gd}=2$, we obtain for the exchange and molecular field $B^{ex}=B^{m}=(380\pm9)$ T. The interpretation of our result with eqn. (1) requires the input of the Fe spin. If we take from [14] the value $S_{Fe}=1.02$, we obtain for the exchange constant $\mathcal{J}_{GdFe}=(1.80\pm0.04)$ meV. This value agrees rather well with the values of $\mathcal{J}_{GdFe}$ deduced from "free powder" high field magnetization data (1.89 meV) [15] and obtained from *ab initio* band structure calculations (1.90 meV) [14] but it is considerably lower compared to earlier band structure calculations

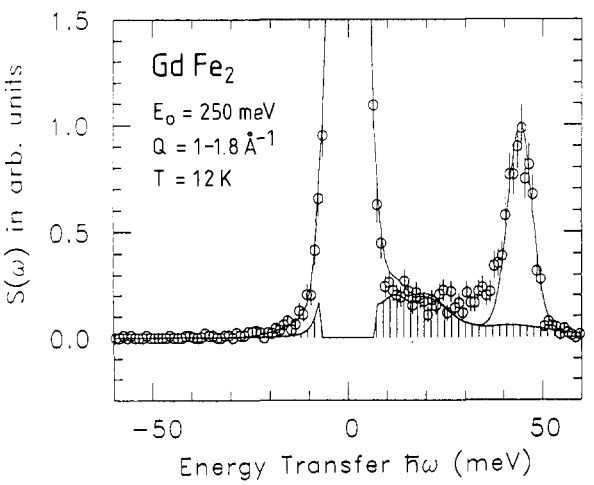

Fig. 5. Inelastic neutron spectrum of $GdFe_2$ at $T=12$ K. The hatched area indicates non-magnetic inelastic intensity as deduced from the spectrum at high Q-values [13].

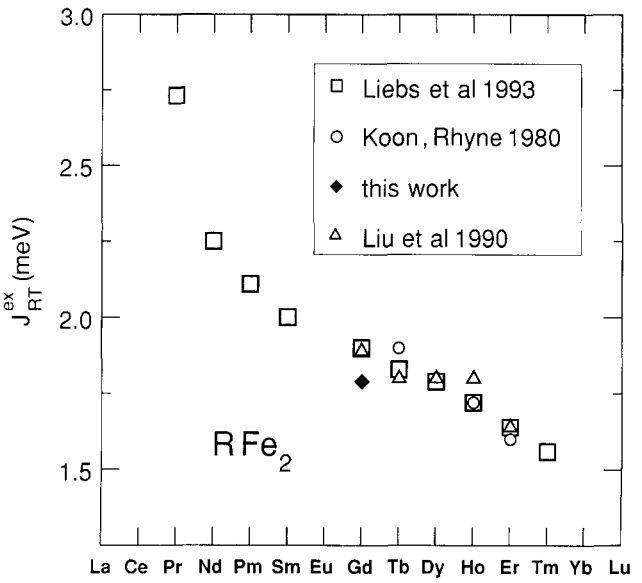

Fig. 6. R–T exchange constants for the series RFe_2 as determined from inelastic neutron data [10; and this work], high-field magnetization data [15] and obtained from band structure calculations [14].

(2.4 meV) [16]. In Fig. 6, we present the results for $\mathcal{J}^{ex}_{RT}$ for the whole series RFe_2 from inelastic neutron scattering experiments for R = Tb, Ho, Ti, Er [10] and Gd (this work), from "free powder" data [15] and from theoretical calculations [14]. We can state that for this simple model system, there is an excellent agreement between experiment and theory within a few percent.

4. $R_2Fe_{14}B$, a complex system

Finally, we discuss the technically interesting, but very complicated $R_2Fe_{14}B$ compounds. They crystallize in a tetragonal structure with space group $P4_2/mnm$ with four formula units in the unit cell. This would lead to 64 spin wave modes, which are, of course, beyond any chance of being determined experimentally. Furthermore, the R-ions occupy the special positions (4f) and (4g) with the low local symmetry requiring two sets of nine CF-parameters for the description of the crystal field. There have been many attempts to determine the full set of CF-parameters experimentally and theoretically (for a survey, see *e.g.* ref. 17). We think, however, that the given sets are still far from being correct except for the leading B_{20} parameter. But even for this parameter, only the site-averaged value is known with some accuracy while the exact values for the different sites are still a matter of controversy.

To simplify the description of the spin dynamics, we first consider $Y_2Fe_{14}B$ with non-magnetic R = Y. Here we expect only one low-lying highly dispersive acoustic

mode, *e.g.* the Fe–Fe mode in fig. 4 with a small gap at the Γ-point corresponding to the small Fe-anisotropy. This mode has been observed in an inelastic neutron scattering experiment on a single crystal [18]. For $Gd_2Fe_{14}B$, we expect two additional low lying modes: a flat R–R mode and a weakly dispersive R–Fe mode. The flat mode can again be easily identified in the magnetic excitation spectrum of a polycrystalline sample of $Gd_2Fe_{14}B$ employing neutrons of an incident energy of $E_0 = 250$ meV [19]. From the energy of the flat mode (37.5 meV), one can directly deduce the exchange field using eqn. (2): $H^{ex} = 324$ T. With $S_T = 1.17$ [20] and $z_{RT} = 16$, we obtain for the exchange constant $\mathcal{J}_{RT} = (1.00 \pm 0.05)$ meV. This is again in excellent agreement with the theoretical value of 1.01 meV [14,21].

The temperature dependence of the excitation spectra of $Gd_2Fe_{14}B$ has been measured under the same conditions [22]. The spectra at 20 K and 300 K are shown in Fig. 7. There is a small shift of the flat-mode peak position with temperature which can be understood by the temperature dependence of $\langle S_T \rangle$ (for finite temperatures we have to take the thermal average of S_T in eqn. (1)).

Before we discuss the results of B^{ex} or $\mathcal{J}^{ex}$ for the whole $R_2Fe_{14}B$ series, we will try to give an explanation for some less pronounced features of the excitation spectra of $Gd_2Fe_{14}B$. At 20 K, there is a shoulder at the low-energy side of the flat-mode peak. While for increasing temperature the main peak moves to slightly lower energies, the shoulder does the opposite; it moves to slightly higher energies towards the main peak. We think that the shoulder originates from another characteristic feature of our simple model as sketched in Fig. 4, *i.e.* the gap of the upper dispersive magnon branch. For the isotropic case, the gap of the lower branch is zero while the energy Δ^+ of the upper branch at the Γ-point is given by

$$\Delta^+ = 2z_{RT}\mathcal{J}_{RT}|S_T - S_R N_R/N_T| \qquad (3)$$

with N_T and N_R the number of T and R-ions in the unit cell (for $R_2Fe_{14}B$, $N_R/N_T = 1/7$) and $S_R = 7/2$ for Gd. With $S_T = 1.17$ and $\mathcal{J}_{RT} = 1.0$ meV (see above), we obtain $\Delta^+ = 21.3$ meV, which is in surprisingly good agreement with the position of the shoulder at 20 K. As $\langle S_R \rangle$ decreases much faster with temperature than $\langle S_T \rangle$, we expect first an increase in Δ^+ with increasing temperature as seen in Fig. 7. For even higher temperatures Δ^+ should pass a maximum and collapse to zero energy at the Curie temperature.

If we apply eqn. (3) to the situation in $GdFe_2$, we obtain $\Delta^+ = 31.5$ meV which might explain the extra intensity at this energy in the spectrum of Fig. 5. Comparing the situation of $GdFe_2$ and $Gd_2Fe_{14}B$, however, we want to mention that the value $(S_T - S_R N_R/N_T)$ is negative for the first compound and positive for the second compound. This leads to a modification of Fig. 4 when applied to the $R_2Fe_{14}B$ series. The highly dispersive Fe–Fe mode now starts at a lower energy than the R–Fe mode with moderate dispersion. If we accept this modified picture, we can also understand why the only dispersive mode observed up to now in a $Nd_2Fe_{14}B$ single crystal [18] has nearly the same spin wave stiffness constant as the highly dispersive mode in $Y_2Fe_{14}B$. This means that the dispersive mode as observed in both compounds (for R = Y and Nd) must be interpreted as the Fe–Fe mode.

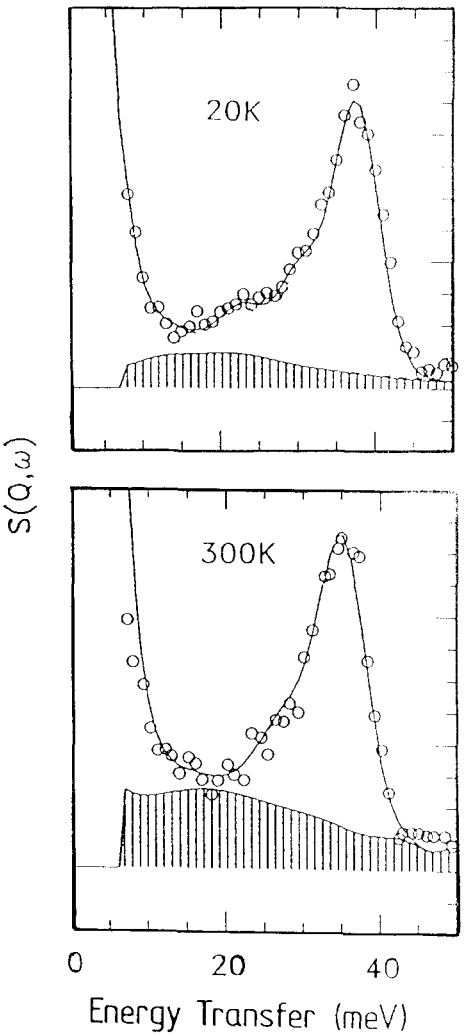

Fig. 7. Inelastic neutron spectra of $Gd_2Fe_{14}B$ at $T = 20$ K and 300 K obtained with $E_0 = 250$ meV for low Q-values. The hatched area indicates non-magnetic inelastic intensity as deduced from the spectra at high Q-values [22].

We now come to the discussion of the rather complex excitation spectra of polycrystalline samples of the whole $R_2Fe_{14}B$ series [23,24]. Here the flat modes exhibit one-, two- and even three-peaked structures depending on the R-ion. In addition, there are shoulders and low-intensity side peaks. A unique interpretation is still

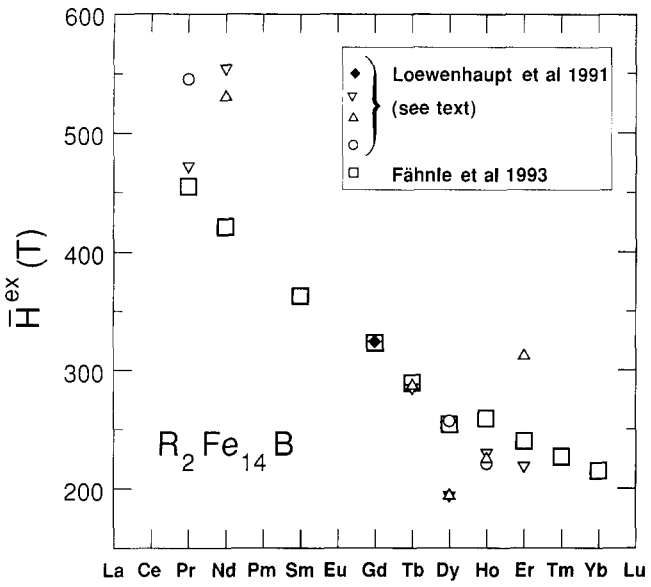

Fig. 8. Average R–T exchange fields for the series $R_2Fe_{14}B$ as determined from inelastic neutron data [24] for R = Gd (◆) and for the other R ions using different sets of CF-parameters: Yamada *et al.* [25] (▽), Givord *et al.* [26] (△) and Radwanski *et al.* [27] (○). Also shown are the values obtained from band structure calculations [21].

missing. For example, the two equally intense main peaks of the excitation spectrum of $Tb_2Fe_{14}B$ can be interpreted as arising either from two different exchange fields or from two different crystal fields at the two R-sites or from a combination of both. Neglecting the details of the structure of the flat-mode peaks, however, we can determine the average exchange field $\bar{H}^{ex}$ from the average position of the dominant peaks. These average exchange fields are shown in Fig. 8 together with theoretical results. Our experimental results for $\bar{H}^{ex}$ of course, depend on the choice of CF-parameters which, on the other hand, cannot be determined from the neutron spectra. We therefore use different sets of CF-parameters from different groups (which are mainly derived from high-field magnetization data of single crystals) and mark the values of $\bar{H}^{ex}$ for each R-ion accordingly with different symbols in Fig. 8. The exception is again R = Gd where crystal field effects are unimportant for the interpretation of the neutron data. As already observed for the RFe_2 series, we find rather good agreement between experimental and theoretical values. The latter may even serve as input to identify the correct CF-parameters that have to be used for the interpretation of the data.

Acknowledgments

We are indebted to Professors I. Sosnowska and M. Fähnle for stimulating discussions and to Drs. T. Perring, R. Eccleston and A. Taylor from ISIS (Rutherford Appleton Laboratories) for valuable assistance during the experiments on the Gd–Fe compounds.

References

1 M. Sagawa, S. Fujimura, N. Togawa, H. Yamamoto and Y. Matsuura, *J. Appl. Phys., 55* (1984) 2083.
2 M. Loewenhaupt, *Physica B, 163* (1990) 479.
3 E. Gratz, M. Loewenhaupt, M. Divis, W. Steiner, E. Bauer, N. Pillmayr, H. Müller, H. Novotny and B. Frick, *J. Phys.: Condensed Matter, 3* (1991) 9297.
4 K.W.H. Stevens, *Proc. Phys. Soc. A, 65* (1952) 209.
5 M.T. Hutchings, in F. Seitz and B. Turnbull (eds.), *Solid State Physics*, Vol. 16, Academic Press, New York, 1964, p. 227.
6 P. Fulde, in K.A. Gschneidner, Jr. and L. Eyring (eds.), *Handbook on the Physics and Chemistry of Rare Earths*, Vol. 2, North-Holland, Amsterdam, 1978, p. 295.
7 P. Fulde and M. Loewenhaupt, *Adv. Phys., 34* (1985) 589.
8 U. Walter, *J. Phys. Chem. Solids, 45* (1984) 401.
9 P. Hoffmann, *J. Phys. A: Math. Gen., 24* (1991) 35.
10 N.C. Koon and J.J. Rhyne, in J.E Crow, R.P. Guertin and T. Mihalisin (eds.), *Crystalline Electric Field and Structural Effects in f-Electron Systems*, Plenum, New York, 1980, p. 125.
11 K. Clausen, J.J. Rhyne, B. Lebech and N.C. Koon, *J. Phys. C: Solid State Phys., 15* (1982) 3587.
12 J.J. Rhyne, *J. Magn. Magn. Mater., 70* (1987) 88.
13 M. Loewenhaupt, P. Fabi, R. Eccleston and T. Perring, ISIS Experimental Report for RB 3182, 1993, p. A254.
14 M. Liebs, K. Hummler and M. Fähnle, *J. Magn. Magn. Mater., 124* (1993) 239, and private communication.
15 J.P. Liu, F.R. de Boer and K.H.J. Buschow, *J. Magn. Magn. Mater., 98* (1991) 291.
16 M.S.S. Brooks, T. Gasche, S. Auluck, L. Nordström, L. Severin, J. Trygg and B. Johansson, *J. Appl. Phys., 70* (1991) 5972.
17 G.J. Long and F. Grandjean (eds.), *Supermagnets, Hard Magnetic Materials*, Kluwer, Dordrecht, 1991.
18 H.M. Mayer, M. Steiner, N. Stüsser, H. Weinfurter, B. Dorner, P.A. Lindgård, K.N. Clausen, S. Hoek and R. Verhoef, *J. Magn. Magn. Mater., 104–107* (1992) 1295.
19 M. Loewenhaupt, I. Sosnowska, A. Taylor and R. Osborn, *J. Appl. Phys., 69* (1991) 5593.
20 K. Hummler, T. Beuerle and M. Fähnle, *J. Magn. Magn. Mater., 115* (1992) 207.
21 M. Fähnle, K. Hummler, M. Liebs and T. Beuerle, *Appl. Phys., A57* (1993) 67.
22 M. Loewenhaupt, P. Hoffmann and A. Taylor, ISIS Experimental Report for RB 2338, 1992, p. A236.
23 M. Loewenhaupt, I. Sosnowska and B. Frick, *Phys. Rev. B, 42* (1990) 3866.
24 M. Loewenhaupt and I. Sosnowska, *J. Appl. Phys., 70* (1991) 5967.
25 M. Yamada, H. Kato, H. Yamamoto and Y. Nakagawa, *Phys. Rev. B, 38* (1988) 620.
26 D. Givord, H.S. Li, J.M. Cadogan, J.M.D. Coey, J.P. Gavigan, O. Yamada, H. Maruyama, M. Sagawa and S. Hirosawa, *J. Appl. Phys., 63* (1988) 3713.
27 R.J. Radwanski and J.J.M. Franse, *J. Magn. Magn. Mater., 80* (1989) 779.